

Article

Analysis, Design, and Control of a Novel Elastomeric Bearing Positioning Stage

Yen-Chu Teng * and Kuo-Shen Chen

Department of Mechanical Engineering, National Cheng-Kung University, Tainan 70101, Taiwan; kschen@mail.ncku.edu.tw

* Correspondence: j0123456jjj@gmail.com; Tel.: +886-6-275-7575 (ext. 62192)

Academic Editor: Chien-Hung Liu

Received: 20 July 2016; Accepted: 22 August 2016; Published: 1 September 2016

Abstract: As products are required with higher precision, vibration control becomes more important for precision machining and inspection. A stage with both fast positioning and relative vibration eliminated can improve product quality. Elastomeric bearings are widely used in the seismic engineering and precision machining fields. By utilizing their stiffness anisotropy, miniaturized bearings can be made of rubbers and have the same function as much larger compliant mechanism-based designs. This provides possible advantages in precision positioning. In this paper, to model the system dynamics of the stage, the mechanical properties of elastomeric bearings are determined through essential material tests of the load cells in this system. The results show that the bearing stiffness is both frequency- and time-dependent. A single-degree-of-freedom precision stage containing four elastomeric bearings is then designed and realized. The stiffness of the elastomeric bearings is modeled as a generalized Maxwell model by system dynamics testing of the controller design. A closed-loop control system comprising an AVM40-20 voice coil motor, an ASP-10-CTR capacitance probe, and an Integral Sliding Mode controller is proposed for the precision stage. Signal processing for the entire system is performed under an NI cRIO-9014 LabVIEW field-programmable gate array real-time controller. In comparison with a previous compliant mechanism-based design, the stage size is reduced from $130 \times 40 \times 15 \text{ mm}^3$ to $30 \times 33 \times 33 \text{ mm}^3$, the positioning stroke is increased from 101 to 139 μm , and the bandwidth is increased from 29 to 350 Hz.

Keywords: elastomeric bearings; generalized Maxwell model; positioning stage; controller design

1. Introduction

As requirements of product accuracy become more serious, vibration control in precision machining [1] and inspections [2] become more important. In order to achieve vibration suppression and isolation, adequate feedback controls also need to be implemented [3,4]. Precision positioning stages that provide high-speed positioning and control capabilities are a method to solve the above-mentioned vibration problems for improving machine performance and product qualities.

Traditionally, compliant stages actuated by piezoelectric (PZT) actuators are typical designs for achieving vibration control. For example, Chang and Du [5] designed a micropositioning stage with a stroke of 100 μm and a resolution of 0.04 μm . Wang and Lee [6] developed a single-degree-of-freedom PZT compliant positioning stage for automatic optical inspection (AOI) applications. It can provide a maximum stroke of 101 μm with a 53.8 nm steady state error and a bandwidth of 29 Hz. Wang and Lee [6] further extended their design to form a stacked two-degree-of-freedom PZT compliant positioning stage.

Compliant mechanisms usually have complicated shapes and large volumes for specific mechanical designs. When the design purpose is changed, the compliant mechanism must be

redesigned. However, its large volume may impose limits on the design. Elastomeric bearings—which are flexible with regard to stiffness design—are another good choice for mechanical design.

Previously, Cuff [7] developed a single-degree-of-freedom electromagnetic nanopositioner with elastomeric bearings that provides a 100 μm stroke and 580 Hz bandwidth. Kluk [8] developed an advanced fast steering mirror for optical communication with elastomeric bearings that provides 3.5 mrad angular motion and 10 kHz bandwidth. These are typical examples of elastomeric bearings in precision stage control.

However, elastomers are viscoelastic materials, which means that their stiffness is time- and frequency-dependent. Without adequate system modeling, an elastomeric-bearing stage may not be adequately controlled. One can refer to Gent's book [9] for rubber engineering and previous works on dealing with the constitutive behaviors of elastomers for a review of the basic concepts in their mechanical properties. For example, see [10–15]. In previous works [7,8], researchers used linear elastic models to model the mechanical behavior of elastomers. On the contrary, elastomeric bearings are modeled as viscoelastic materials in this work, and associated controllers are designed. By this approach, it is expected that the advantages and superiority of elastomeric bearing stages can be fully realized.

The rest of this article presents the work in detail. In Section 2.1, the conceptual design of the overall system is presented. The design of the elastomeric bearing is presented in Section 2.2. In Section 2.3, the mathematical model of the bearing is derived, and several tests are applied to figure out the characteristics of the bearing and the voice coil motor. The design and implementation of the controller design are presented in Section 2.4. The positioning experiments are presented in Section 3. Essential discussions are provided in Section 4. Finally, Section 5 concludes the paper.

2. Methods

2.1. Approach

The research flow of this work is shown in Figure 1. The first issue is to perform mechanical analysis and design of the stage body, followed by basic dynamic testing to obtain the system model. With proper integration of the sensor and actuator, the controller design is then investigated in order to evaluate the performance and quality of the design.

In this paper, instead of using compliant structures, elastomeric bearings are used to provide stiffness and control the dynamic behavior of the proposed precision positioning stage. An elastomeric material (silicone) is chosen for the elastomeric bearings. First, the shape and size of the bearings are designed by considering the stiffness and natural frequencies of the stage. A viscoelastic model is applied to model the stiffness of the elastomeric bearings. Then, several system dynamics experiments are performed to find the parameters of the viscoelastic model.

The main purpose of the stage is single-degree-of-freedom precision positioning with a motion stroke of 100 μm . The system—shown schematically in Figure 2—contains an AVM40-20 voice coil motor (bandwidth 2000 Hz, peak actuating force 29 N) for actuation, an ASP-10-CTR capacitive probe, an aluminum block with four elastomeric pads as rubber bearings, and a LabVIEW field-programmable gate array (FPGA) controller to control the motion. The voice coil motor actuates the stage and the capacitive probe for movement sensing. The design exploits the deformation of the elastomeric bearing to provide essential structural stiffness, and the overall performance is a compromise between desired specifications, static and dynamic responses, and controllability considerations. The ASP-10-CTR capacitive probe has a measurement range of 254 μm , a resolution of 10 nm, and a bandwidth of 1 kHz, and is extremely suitable for this design. Meanwhile, to investigate the mechanical properties and for pre-load adjustment of the elastomeric bearings, one LM-10 and two S-100 load cells were also mounted on the experiment structure to observe the loading on the elastomeric bearings and the force transmitted from the voice coil motor. Notice that the selection of sensor and actuator in this work is not unique but is based on the compromise between performance, cost, and system integration

factors. For example, it is also possible to use a piezoelectric (PZT) actuator [6,16] or a magnetostrictive actuator [16] in this design. However, in comparison with voice coil motors at the same characteristic length, the stroke of PZT actuators is usually much less, and the magnetostrictive actuators are much heavier—neither of them can satisfy the design goal. The entire control flow is shown in Figure 3.

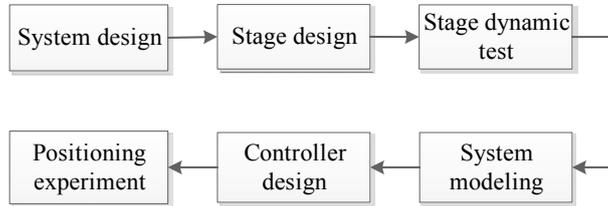


Figure 1. System research flow diagram.

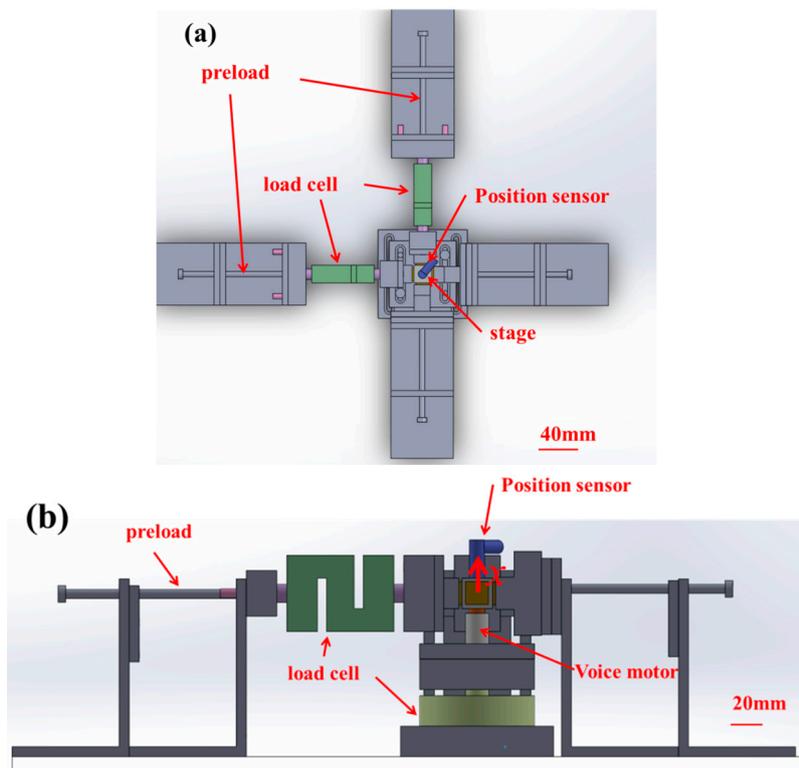


Figure 2. Schematic diagram of the experimental setup. (a) top view of the stage, which is the part of the green box in (b) and (b) front view of the entire setup. x indicates the motion direction.

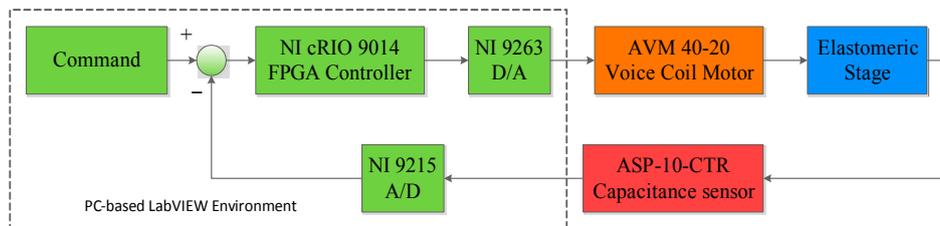


Figure 3. Block diagram for the control system.

2.2. Stage Design and Realization

As shown schematically in Figure 4, the stage mainly included an aluminum block and four silicone elastomeric bearings attached to it. To conduct the mechanical analysis in order to determine the system stiffness, this work follows a similar flow to [7], based on the textbook content of [9], before considering the viscoelastic effect. The stiffness in the positioning (z -axis) direction, k_z , can be expressed as the combined shear stiffness (i.e., k_s , shown below) of all four bearings. On the other hand, the stiffness of the other two axes (x - and y -axes), k_x and k_y , can be modelled as the combined stiffness (i.e., k_c , shown below) of two k_s and two k_c stiffnesses of individual bearings. Although rubbers are nonlinear materials, they behave linearly under small strain conditions. In terms of linear elasticity, k_z is proportional to the stage stroke, and the natural frequency of the stage strongly depends on k_z . On the other hand, since the design has a single degree of freedom, k_x and k_y should be much larger than k_z . In this work, a ratio of 10 is used for structural design, such that the motions in both in-plane degrees of freedom (i.e., x and y) are much stiffer than that in the out-of-plane direction (i.e., z -direction) to ensure the single degree of freedom approximation.

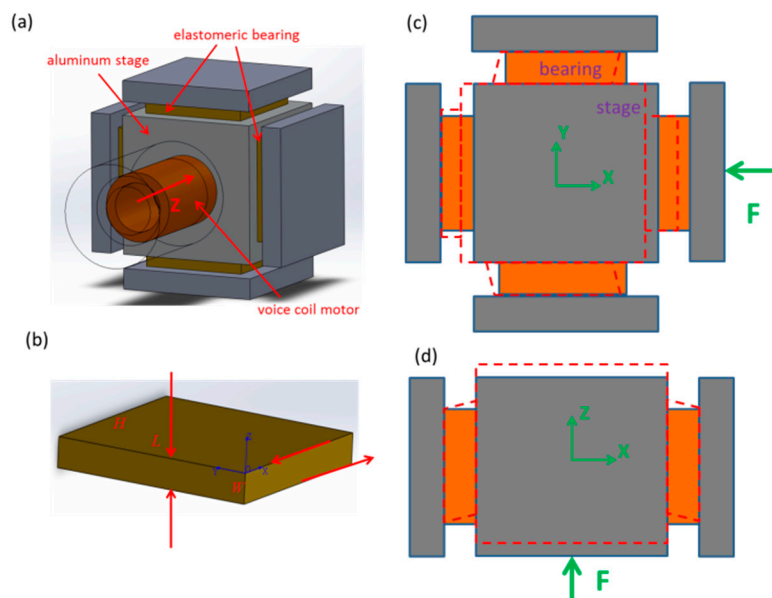


Figure 4. (a) Schematic plot of the stage; (b) dimensions (L : length, H : width, and W : thickness) and coordinates of the elastomeric bearings. Schematic plots indicating (c) in-plane and (d) out-of-plane motion. The dashed lines in (c,d) indicate the deformed shape subjected to a force F .

The compression modulus, E_c , of the elastomeric bearings is strongly related to their shape factor S , and one can modify their geometry to adjust k_c . On the other hand, the shear modulus is $1/3$ of the Young’s modulus E_0 . In this work, by evaluating all these issues, the dimensions of the bearing and stage are finally designed to be four $15 \times 15 \times 1.5 \text{ mm}^3$ (silicone) elastomeric bearings and a $30 \times 30 \times 30 \text{ mm}^3$ aluminum stage, respectively. The experimental system is realized as shown in Figure 5.

The stiffness of the elastomeric bearing is related to the elastic modulus and shape factors, and can be expressed as [7,10] for a rubber pad with length L , width H , and thickness W :

$$\text{For compression, } E_c = E_0(1 + 2\kappa S^2) \Rightarrow k_c = \frac{E_c LH}{W} ; \tag{1}$$

$$\text{For shear, } G = \frac{E_0}{3} \Rightarrow k_s = \frac{GLH}{W} , \tag{2}$$

where

$$S = \frac{LH}{2W(L + H)} \tag{3}$$

From Equations (1) and (2), the stiffnesses k_x , k_y , and k_z of the x -, y -, and z -axes are 4.10, 4.10, and 0.36 N/ μ m, respectively. The natural frequencies of the x , y , and z -axes are 864, 864, and 256 Hz. The maximum output force of the voice coil motor is 27 N, and the corresponding maximum stroke is 150 μ m.

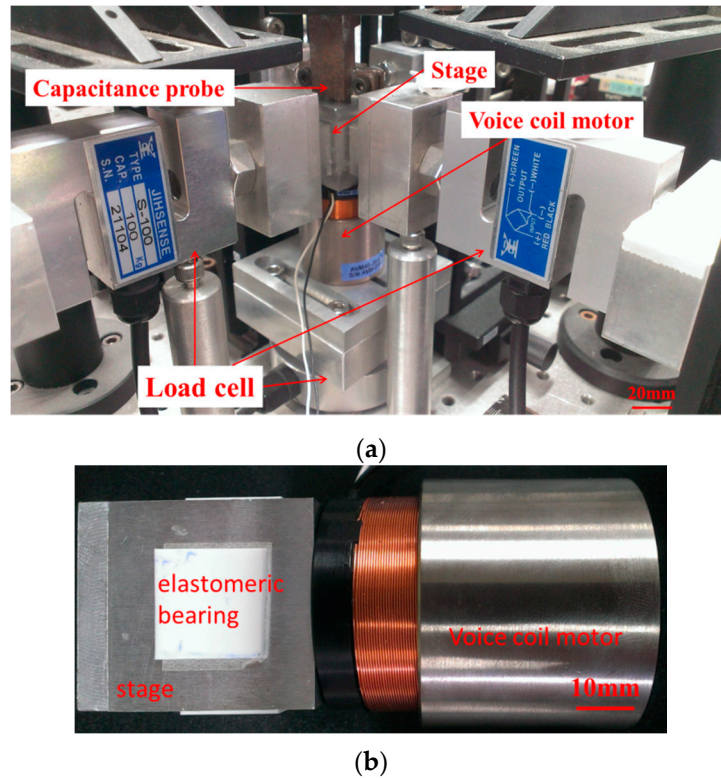


Figure 5. Experimental system setup. (a) The picture of the entire system; (b) the stage and voice coil assembly.

2.3. Dynamic Testing and Modeling of the Stage

2.3.1. Stage Model

The stage is modeled as a single-degree-of-freedom vibration system (shown in Figure 6a) with a mass M , a damper with damping coefficient C , and a time- and frequency-varying spring $K(s)$, which is mainly caused by the viscoelastic effect of the elastomeric materials. It is modelled by using a generalized Maxwell model [17] with two dampers, c_1 and c_2 , and three linear springs, k_1 , k_2 , and k_3 , shown schematically in Figure 6b. Notice that there are no distinctive physical dampers installed in the experimental system. The equivalent damping considered in the stage model actually comes from the material damping of the elastomers and the magnetic damping from the voice coil actuator. By force equilibrium, it can be shown that the transfer function, $K(s)$, of this stiffness element can be expressed as:

$$K(s) = \frac{\alpha s^2 + \gamma s + k_1 k_2 k_3}{c_2 c_3 s^2 + (k_2 c_3 + c_2 k_3) s + k_2 k_3}, \tag{4}$$

where

$$\alpha = k_1 c_2 c_3 + k_2 c_2 c_3 + c_2 c_3 k_3 \tag{5}$$

$$\gamma = k_1 k_2 c_3 + k_1 c_2 k_3 + c_2 k_2 k_3 + k_2 k_3 c_3. \tag{6}$$

The mass M of the model is taken as the mass of the aluminum stage and the coil of the voice coil motor, 139 g, since the mass of the four elastomeric bearings is negligible in comparison with that of the stage. The damping coefficient C is difficult to obtain analytically, and is experimentally determined by examining the open-loop step response. All model parameters are listed in Table 1. The entire stage transfer function can thus be expressed as:

$$G_s(s) = \frac{X}{F} = \frac{1}{Ms^2 + Cs + K(s)}. \tag{7}$$

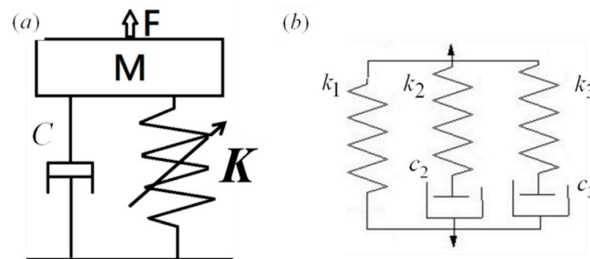


Figure 6. (a) Stage model with a modal mass M , damping C , and a varying stiffness K ; (b) Viscoelastic model of stage stiffness with stiffness k_1, k_2, k_3 and dampings c_2 and c_3 . Please refer to Table 1 for their definitions.

Table 1. Fundamental design parameters of the system.

C (N·s/m)	k_1 (N/m)	k_2 (N/m)	k_3 (N/m)	c_2 (N·s/m)	c_3 (N·s/m)
800	3.86×10^5	6.3×10^4	4.4×10^4	504	101,200

2.3.2. Stress Relaxation Experiment

Using a stress relaxation test, the time history of the stiffness under a given initial fixed displacement can be obtained, and is shown in Figure 7. By using a Prony series approach, the stiffness can be fitted in the following form:

$$K(t) = k_1 + k_2e^{-k_2t/c_2} + k_3e^{-k_3t/c_3}. \tag{8}$$

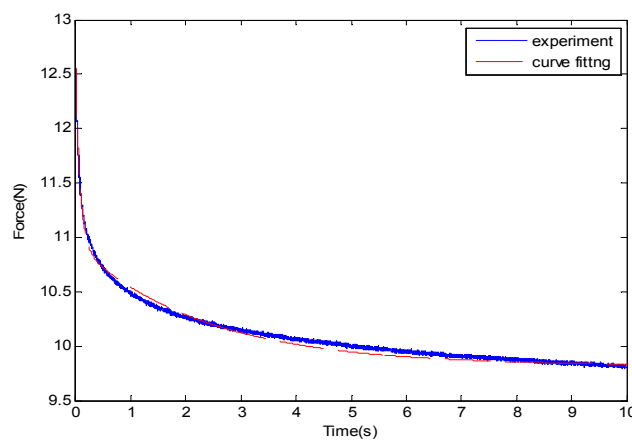


Figure 7. Stress relaxation experiment results.

The parameters in Equation (4) and shown in Table 1 can be obtained once the curve fitting of Equation (8) is determined.

2.3.3. Damping Coefficient Experiment

A comparison of the simulation and the experimental results of the open-loop step response of the stage is shown in Figure 8. The experimental data can be treated as the contribution of two major sources. That is, a slow rising part and an oscillation part. The vibration frequency of the oscillation part is about 140 Hz, which differs from the natural frequency of the stage. We believe that this is possibly due to the vibration of the auxiliary supporting structure for providing preloads, and should not be counted in the system dynamics of the stage. By adjusting the damping coefficient in the associated stage dynamics and performing curve fitting, the damping coefficient C that can be obtained is about 800 N·s/m, the damping ratio is 1.5, and the stage should be overdamped.

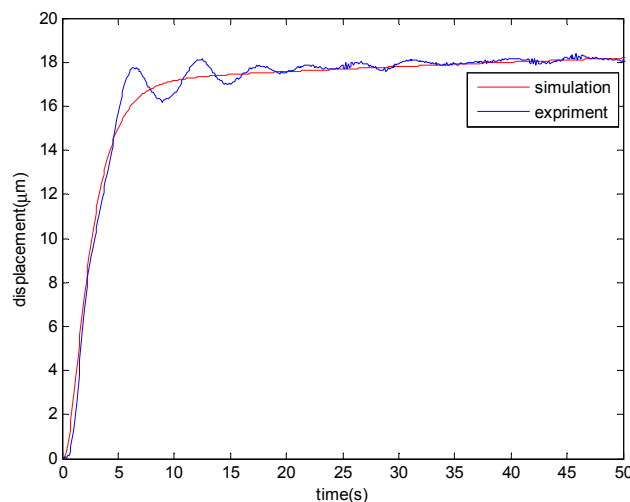


Figure 8. Open-loop step response.

2.4. Controller Design

The actuator contains a power amplifier and a voice coil motor. The bandwidth of the amplifier (200 Hz) is much smaller than that of the actuator itself (i.e., 2000 Hz). Using system dynamics, the power amplifier and the voice coil motor can be modeled as a first-order system. On the other hand, the elastomeric bearing stage is a fourth-order system by Equations (4) and (7). Therefore, the entire plant is a fifth-order system. However, this full model is too complicated; thus, the model is simplified to be a third-order model in which is contained a first-order actuator model and a second-order stage model (which is a normal vibration model with a constant stiffness) as a reference model for controller design. Although the controller design in this paper is based on simplified dynamics, the original fifth-order model can still provide important information. That is, it provides a reasonable measurement to model the stiffness uncertainty, which is critical for the determination of control parameters in sliding mode controller (SMC) design. In addition, the full fifth-order model will be used to design the controller in the near future.

2.4.1. Proportional–Integral–Derivative (PID) Controller

A traditional PID controller is designed under a 10 kHz loop rate in this paper for the initial evaluation of system performance, and as a basis for the comparison of the effectiveness of more advanced controllers. The transfer function of the PID controller [18] may be expressed as:

$$G_c(s) = K_p \left(1 + \frac{T_i}{s} + T_d s \right), \quad (9)$$

where K_p , T_i , and T_d are the gains for proportional, integration, and derivative gains, respectively.

2.4.2. Integral Sliding Mode Controller

Sliding Mode Control [19] is a nonlinear control design and has a robust control effect on the system parameter uncertainty. Integral Sliding Mode Control (ISMC) [20] is based on SMC, where an error integral term is added to the sliding function $s(x)$ (as shown in Equation (10)) to increase the convergence of errors. When the system state is on the sliding surface, $\dot{s} = 0$ is applied to derive the controlled input, as in Equations (11) to (15). The switching input u_n is designed to have a compensation term Δf included to represent the parameter uncertainty. The time- and frequency-varying stiffness is regarded as the parameter uncertainty of the stage, as in Equation (15). The design of the stiffness uncertainty Δk is based on the stress relaxation experiment in Section 2.3.2.

$$s(x, t) = \left(\frac{d}{dt} + \lambda \right)^{n-1} (x(t) - x_d(t)) + \beta \int_0^t (x(t) - x_d(t)) \quad (10)$$

$$\dot{s}(x, t) = \ddot{\tilde{x}} + \lambda \dot{\tilde{x}} + \beta \tilde{x} = \ddot{x} - \ddot{x}_d + \lambda \dot{\tilde{x}} + \beta \tilde{x} = f + u - \ddot{x}_d + \lambda \dot{\tilde{x}} + \beta \tilde{x} \quad (11)$$

$$u = u_{eq} + u_n \quad (12)$$

$$u_{eq} = -f + \ddot{x}_d - \lambda \dot{\tilde{x}} - \beta \tilde{x} \quad (13)$$

$$u_n = -(|\Delta f| + \eta) \text{sat}(s, \phi), \quad (14)$$

where

$$\Delta f = \frac{\Delta k}{M} \tilde{x}. \quad (15)$$

Based on the Lyapunov stability theorem, $V(s)$ is chosen as the Lyapunov function, as shown in Equation (16). According to the derivation shown in Equation (17), the constant η must be positive:

$$V(s) = \frac{1}{2} s^2 \quad (16)$$

$$\begin{aligned} \dot{V}(s) < 0 &\rightarrow \frac{1}{2} \frac{d}{dt} s^2 = s \dot{s} \\ &= s(f + u - \ddot{x}_d + \lambda \dot{\tilde{x}} + \beta \tilde{x}) \\ &= s(f + u_{eq} + u_n - \ddot{x}_d + \lambda \dot{\tilde{x}} + \beta \tilde{x}) \\ &= s(-|\Delta f| + \eta) \text{sat}(s, \phi) = -(|\Delta f| + \eta) < 0. \end{aligned} \quad (17)$$

3. Results

3.1. Step Response

Typical control results are shown in Figure 9 for a 25.4 μm step command. It can be seen that the open-loop response, although it rises fast initially, cannot reach the destination in a reasonable time. Notice that it finally reaches the destination after 10 s by creeping due to the time-dependent stiffness. On the other hand, the feedback control response shows a significant improvement. The PID controller with a gain set of $K_p = 15$, $T_i = 0.0033$, and $T_d = 0.00093$ achieves a rise time and a settling time of 9 and 20 ms, respectively. The ISMC controller with parameter settings of $\beta = 12,000$, $\varphi = 0.0305$, $\lambda = 12,000$, and $\eta = 30$ achieves a rise time and a settling time of 6 ms and 29 ms, respectively. The parameters for the PID controller are first determined by the Zeigler–Nichols (ZN) method and after performing a series of parametric studies. On the other hand, the final parameters for the ISMC controller are chosen by performing a Matlab simulation and on-line adjustment based on the initial model reference design approach.

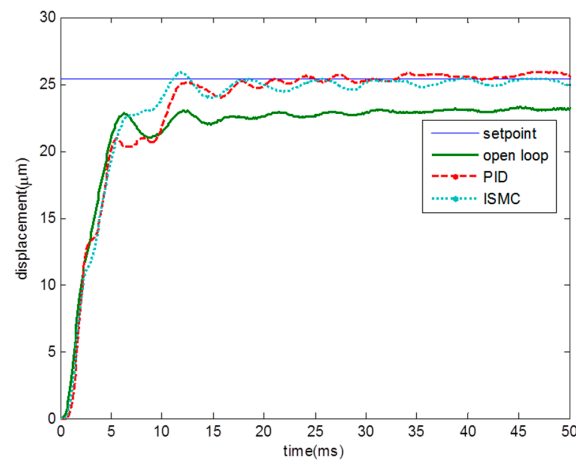


Figure 9. Step responses of the system under different control schemes.

3.2. Sinusoidal Motion Tracking

The sinusoidal tests are performed, and a typical response with 10 Hz actuation is shown in Figure 10. It can be seen that the system response is also significantly improved under PID and ISMC control. Finally, the Bode plot can be obtained with systematic sinusoidal tests, and is shown in Figure 11. The bandwidths of the closed-loop system are approximately 27 and 350 Hz under PID and ISMC controls, respectively.

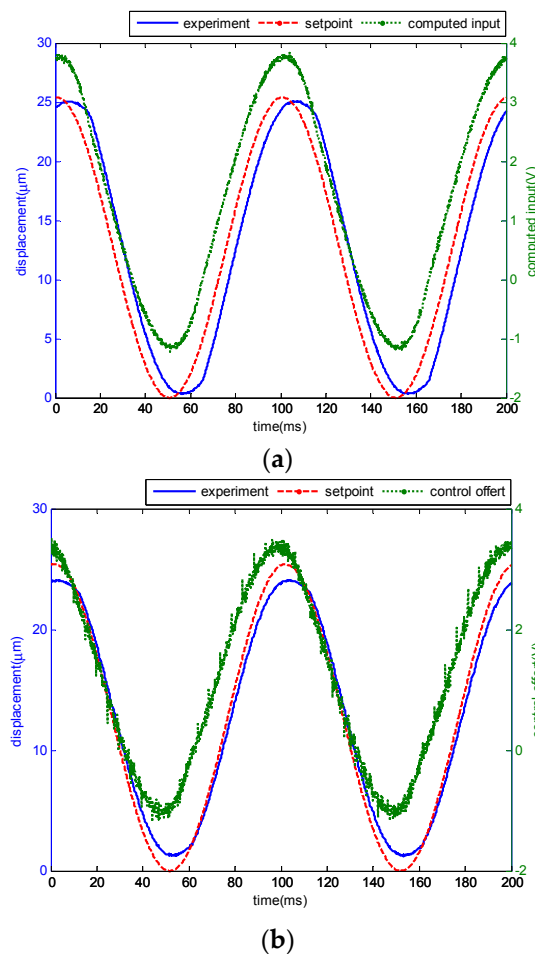


Figure 10. System sinusoidal responses with 10 Hz input under (a) PID and (b) ISMC controls.

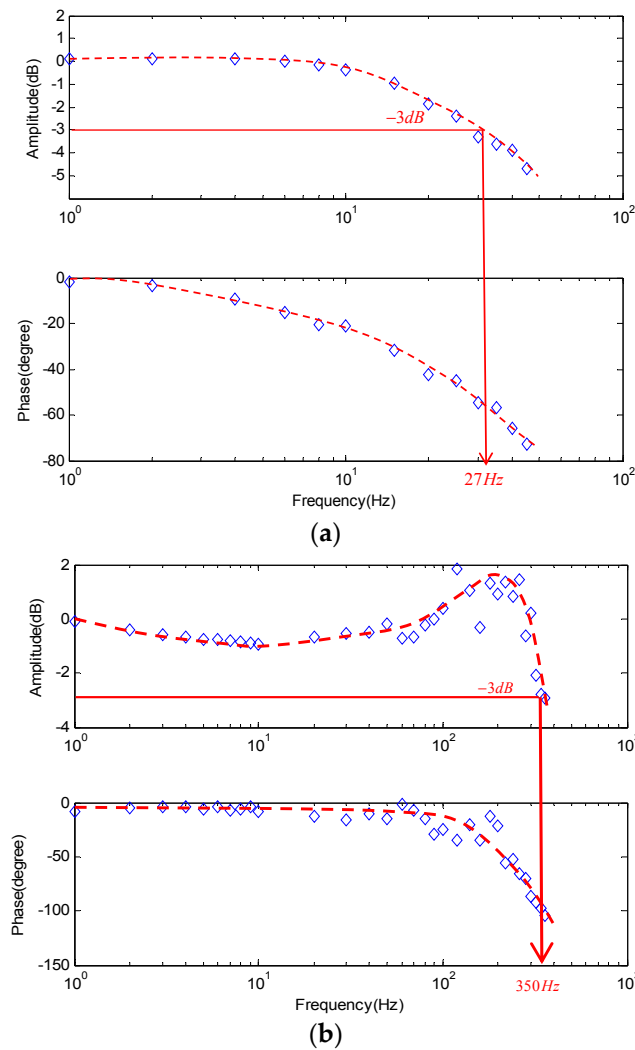


Figure 11. Bode plots of the closed-loop system under (a) PID and (b) ISMC controls.

3.3. Robustness Test

To understand the system robustness, a step response experiment with different loadings was performed. The results in Figure 12 show that there is no obvious change in the system response under different loadings. Therefore, this shows that the system is sufficiently robust to changes in mass.

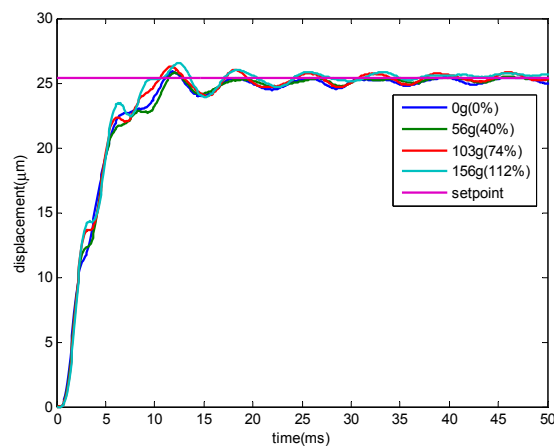


Figure 12. Step response with different loadings.

4. Discussion

In this paper, the design, analysis, and control of an elastomeric-bearing precision positioning stage is presented for possible application in positioning and vibration control for measurement and inspection applications. The system contains an elastomeric bearing stage and is actuated by a voice coil motor. A capacitance probe is used to measure the motion and provide feedback. Finally, a FPGA-based digital controller was designed to perform the motion control.

Due to their viscoelastic nature, the elastomeric bearings were modeled as a generalized Maxwell fluid using the relaxation test data, and the entire stage was modeled as a single-degree-of-freedom system with time- and frequency-varying stiffness. Meanwhile, the actuator was modeled as a first-order system, based on results from associated dynamic tests. The PID and ISMC controllers were designed according to the plant dynamics. The experimental results indicated that the system can achieve bandwidths of 27 Hz and 350 Hz and steady state errors less than 13 nm and 203 nm under PID and ISMC controls, respectively. Table 2 briefly summarizes the performance of the designed system. Notice that in Table 2, the settling time is defined as the time when the tracking error is reduced to be in the range within $\pm 2\%$ of the set-point. Compared with PID control, the system with ISMC has faster positioning speed but worse positioning resolution. The robustness test shows the system has good robustness to changes in the mass. The high damping of the elastomeric bearing system may be the reason for the good system robustness.

Table 2. System performance under PID and ISMC controls.

Performance	PID	ISMC
Steady State Error (nm)	13	203
Overshoot (%)	1.9	2.01
Rise Time (ms)	9	6
Settling Time (ms)	20	29
Bandwidth (Hz)	27	350

Compared to our previous work using compliant mechanisms [4], the size of the elastomeric bearing stage ($30 \times 33 \times 33 \text{ mm}^3$) is smaller than that of the compliant stage ($130 \times 40 \times 15 \text{ mm}^3$). This is a major advantage of incorporating elastomeric bearing design. Such a smaller size represents a major advantage in systems requiring a more compact design. The stroke of the elastomeric bearing stage ($139 \mu\text{m}$) is larger than that of the compliant stage ($101 \mu\text{m}$). The bandwidth of the current design (350 Hz) is also better than that of the previous one (29 Hz). It is expected that, thanks to this work, elastomeric bearing stages can be applied in applications such as automatic inspection machines and precision metrology.

5. Conclusions

In previous works [5,6], researchers used linear elastic models to model the mechanical behavior of elastomers. In this paper, the viscoelastic properties were considered and applied in the system modeling. A stress relaxation test was performed to observe and model the time- and frequency-varying stiffness. Based on the stage model with viscoelastic stiffness, ISMC was designed and realized. The results of the positioning experiment show that this is an effective method for modeling and controlling the elastomeric bearing systems of precision machines.

The full properties of elastomeric bearings are too complicated to be fully modelled. Thus, some properties were not considered in this paper. The compression stress has an effect on the shear stiffness. Considering the relationship between the compression stress and shear stiffness of elastomeric bearings can improve the bearing stiffness design. In addition, the controller design is based on a simplified system model. The performance of the system may improve if the controller design were to be based on the full fifth-order system model.

Acknowledgments: This work was supported by the Ministry of Science and Technology (MOST) of Taiwan under contact numbers NSC 101-2221-E-006-032-MY3. Contributions from Pei Chun Lin and Rong Can Hong of National Cheng-Kung University (NCKU) during the early stages of this work are greatly appreciated. The second author wishes to thanks David L. Trumper of MIT for guiding him into this field.

Author Contributions: Yen-Chu Teng performs the design and control of the stage as a part of his master thesis; Kuo-Shen Chen serves as the thesis supervisor of the first author for conducting this research; He also be responsible for generating the entire idea of this research and conducts preliminary studies for demonstrating the feasibility, as well as for securing the research grants.

Conflicts of Interest: The authors declare no conflict of interest.

References

1. Woronko, A.; Huang, J.; Altintas, Y. Piezoelectric tool actuator for precision machining on conventional CNC turning centers. *Precis. Eng.* **2003**, *27*, 335–345. [[CrossRef](#)]
2. Chang, C.Y.; Li, C.H.; Lin, S.Y.; Jeng, M. Application of Two Hopfield Neural Networks for Automatic Four-Element. *IEEE Trans. Syst. Man Cybern. Part C Appl. Rev.* **2009**, *39*, 352–365. [[CrossRef](#)]
3. Hu, Y.; Chen, M.Z.Q.; Shu, Z.; Huang, L. Analysis and optimization for inerter-based isolators via fixed-point theory and algebraic solution. *J. Sound Vib.* **2015**, *346*, 17–36. [[CrossRef](#)]
4. Hu, Y.; Chen, M.Z.Q.; Xu, S.Y.; Liu, Y. Semi-active inerter and its application in adaptive tuned vibration absorbers. *IEEE Trans. Control Syst. Technol.* **2016**. in press. [[CrossRef](#)]
5. Chang, S.H.; Du, B.C. A precision Piezo driven micropositioner mechanism with large travel range. *Rev. Sci. Instrum.* **1998**, *69*, 1785–1791. [[CrossRef](#)]
6. Wang, W.C.; Lee, J.W.; Chen, K.S. Design and vibration control of a notch-based compliant stage for display panel inspection applications. *J. Sound Vib.* **2014**, *333*, 2701–2718. [[CrossRef](#)]
7. Cuff, D.P. Electromagnetic Nanopositioner. Master's Thesis, Massachusetts Institute of Technology, Cambridge, MA, USA, 2006.
8. Kluk, D.J. An Advanced Fast Steering Mirror for Optical Communication. Master's Thesis, Massachusetts Institute of Technology, Cambridge, MA, USA, 2002.
9. Gent, A.N. *Engineering with Rubber*; Hanser Publications: Cincinnati, OH, USA, 2001.
10. Arruda, E.M.; Boyce, M.C. A three-dimensional constitutive model for the large stretch behavior of rubber elastic materials. *J. Mech. Phys. Solids* **1993**, *41*, 389–412. [[CrossRef](#)]
11. Bergström, J.S.; Boyce, M.C. Constitutive modeling of the large strain time-dependent behavior of elastomers. *J. Mech. Phys. Solids* **1998**, *46*, 931–954. [[CrossRef](#)]
12. Berg, M. A non-linear rubber spring model for rail vehicle dynamics analysis. *Veh. Syst. Dyn.* **1998**, *30*, 197–212. [[CrossRef](#)]
13. Boyce, M.C.; Arruda, E.M. Constitutive models of rubber elasticity: A review. *Rubber Chem. Technol.* **2000**, *73*, 504–523. [[CrossRef](#)]
14. Sjöberg, M.M.; Kari, L. Non-linear behavior of a rubber isolator system using fractional derivatives. *Veh. Syst. Dyn.* **2002**, *37*, 217–236. [[CrossRef](#)]
15. Cao, L.; Sadeghi, F.; Stacke, L.E. An Explicit Finite Element Model to Investigate the Effects of Elastomeric Bushing on Bearing Dynamics. *J. Tribol.* **2016**, *138*, 031104. [[CrossRef](#)]
16. Claeysen, F.; Lhermet, N.; Maillard, T. Magnetostrictive actuators compared to piezoelectric actuators. In *European Workshop on Smart Structures in Engineering and Technology*; International Society for Optics and Photonics: Bellingham, WA, USA, 2003; pp. 194–200.
17. Flügge, W. *Viscoelasticity*; Springer-Verlag: New York, NY, USA, 1975.
18. Ogata, K. *Modern Control Engineering*; Prentice Hall: Upper Saddle River, NJ, USA, 1970.
19. Edwards, C.; Spurgeon, S. *Sliding Mode Control: Theory and Applications*; CRC Press: Boca Raton, FL, USA, 1988.
20. Li, Y.; Xu, Q. Adaptive Sliding Mode Control with Perturbation Estimation and PID Sliding Surface for Motion Tracking of a Piezo-Driven Micromanipulator. *IEEE Trans. Control Syst. Technol.* **2010**, *18*, 798–810. [[CrossRef](#)]

